

Fabrication of phase-change chalcogenide $\text{Ge}_2\text{Sb}_2\text{Te}_5$ patterns by laser-induced forward transfer

Ming Lun Tseng,^{1,2} Bo Han Chen,^{1,2} Cheng Hung Chu,^{1,2} Chia Min Chang,^{1,2} Wei Chih Lin,² Nien-Nan Chu,³ Masud Mansuripur,⁴ Ai Qun Liu,⁵ and Din Ping Tsai^{1,2,3,6,*}

¹Graduate Institute of Applied Physics, National Taiwan University, Taipei 106, Taiwan

²Department of Physics, National Taiwan University, Taipei 106, Taiwan

³Instrument Technology Research Center, National Applied Research Laboratories, Hsinchu 300, Taiwan

⁴College of Optical Sciences, The University of Arizona, Tucson, Arizona 85721, USA

⁵School of Electrical and Electronic Engineering, Nanyang Technological University, 50 Nanyang Avenue, 639798, Singapore

⁶Research Center for Applied Sciences, Academia Sinica, Taipei 115, Taiwan

*dptsai@phys.ntu.edu.tw

Abstract: Femtosecond laser pulses are focused on a thin film of $\text{Ge}_2\text{Sb}_2\text{Te}_5$ phase-change material, and the transfer of the illuminated material to a nearby substrate is investigated. The size, shape, and phase-state of the fabricated pattern can be effectively controlled by the laser fluence and by the thickness of the $\text{Ge}_2\text{Sb}_2\text{Te}_5$ film. Results show multi-level electrical and optical reflection states of the fabricated patterns, which may provide a simple and efficient foundation for patterning future phase-change devices.

©2011 Optical Society of America

OCIS codes: (220.0220) Optical design and fabrication; (310.3840) Materials and process characterization; (210.4810) Optical storage-recording materials.

References

1. S. R. Ovshinsky, "Reversible electrical switching phenomena in disordered structures," *Phys. Rev. Lett.* **21**(20), 1450–1453 (1968).
2. A. L. Greer and N. Mathur, "Materials science: changing face of the chameleon," *Nature* **437**(7063), 1246–1247 (2005).
3. T. Ohta, K. Nishiuchi, K. Narumi, Y. Kitaoka, H. Ishibashi, N. Yamada, and T. Kozaki, "Overview and the future of phase-change optical disk technology," *Jpn. J. Appl. Phys.* **39**(Part 1, No. 2B), 770–774 (2000).
4. K.-F. Kao, C.-M. Lee, M.-J. Chen, M.-J. Tsai, and T.-S. Chin, " $\text{Ga}_2\text{Te}_3\text{Sb}_5$ —A Candidate for Fast and Ultralong retention phase-change memory," *Adv. Mater. (Deerfield Beach Fla.)* **21**(17), 1695–1699 (2009).
5. N. Yamada, E. Ohno, K. Nishiuchi, N. Akahira, and M. Takao, "Rapid-phase transitions of $\text{GeTe-Sb}_2\text{Te}_3$ pseudobinary amorphous thin films for an optical disk memory," *J. Appl. Phys.* **69**(5), 2849–2856 (1991).
6. M. Wuttig and N. Yamada, "Phase-change materials for rewriteable data storage," *Nat. Mater.* **6**(11), 824–832 (2007).
7. M. Terao, T. Morikawa, and T. Ohta, "Electrical phase-change memory: fundamentals and state of the art," *Jpn. J. Appl. Phys.* **48**(8), 080001 (2009).
8. C. B. Peng, L. Cheng, and M. Mansuripur, "Experimental and theoretical investigations of laser-induced crystallization and amorphization in phase-change optical recording media," *J. Appl. Phys.* **82**(9), 4183–4191 (1997).
9. E. M. Wright, P. K. Khulbe, and M. Mansuripur, "Dynamic theory of crystallization in $\text{Ge}_2\text{Sb}_{2.3}\text{Te}_5$ phase-change optical recording media," *Appl. Opt.* **39**(35), 6695–6701 (2000).
10. G. F. Zhou, "Materials aspects in phase change optical recording," *Mater. Sci. Eng. A* **73**, 304–306 (2001).
11. P. Khulbe, E. M. Wright, and M. Mansuripur, "Crystallization behavior of as-deposited, melt-quenched, and primed amorphous states of $\text{Ge}_2\text{Sb}_{2.3}\text{Te}_5$ films," *J. Appl. Phys.* **88**(7), 3926–3933 (2000).
12. R. Pandian, B. J. Kooi, G. Palasantzas, J. T. M. De Hosson, and A. Pauza, "Nanoscale electrolytic switching in phase-change chalcogenide films," *Adv. Mater. (Deerfield Beach Fla.)* **19**(24), 4431–4437 (2007).
13. L. P. Shi, T. C. Chong, P. K. Tan, X. S. Miao, Y. M. Huang, and R. Zhao, "Study of the partial crystallization properties of phase-change optical recording disks," *Jpn. J. Appl. Phys.* **38**(Part 1, No. 3B), 1645–1648 (1999).
14. S. R. Ovshinsky and W. Czubatj, "New developments in optical phase-change memory," *Proc. SPIE* **4085**, 15–22 (2001).
15. D. Lencer, M. Salinga, and M. Wuttig, "Design rules for phase-change materials in data storage applications," *Adv. Mater. (Deerfield Beach Fla.)* **23**(18), 2030–2058 (2011).
16. T. S. Kao, Y. H. Fu, H. W. Hsu, and D. P. Tsai, "Study of the optical response of phase-change recording layer with zinc oxide nanostructured thin film," *J. Microsc.* **229**(3), 561–566 (2008).

17. K. P. Chiu, K. F. Lai, and D. P. Tsai, "Application of surface polariton coupling between nano recording marks to optical data storage," *Opt. Express* **16**(18), 13885–13892 (2008).
18. W. C. Lin, T. S. Kao, H. H. Chang, Y. H. Lin, Y. H. Fu, C. T. Wu, K. H. Chen, and D. P. Tsai, "Study of a super-resolution optical structure: polycarbonate/ZnS-SiO₂/ZnO/ZnS-SiO₂/Ge₂Sb₂Te₅/ZnS-SiO₂," *Jpn. J. Appl. Phys.* **42**(Part 1, No. 2B), 1029–1030 (2003).
19. H. F. Hamann, M. O'Boyle, Y. C. Martin, M. Rooks, and H. K. Wickramasinghe, "Ultra-high-density phase-change storage and memory," *Nat. Mater.* **5**(5), 383–387 (2006).
20. Y. Jung, S. H. Lee, A. T. Jennings, and R. Agarwal, "Core-shell heterostructured phase change nanowire multistate memory," *Nano Lett.* **8**(7), 2056–2062 (2008).
21. Y. Yin, T. Noguchi, H. Ohno, and S. Hosaka, "Programming margin enlargement by material engineering for multilevel storage in phase-change memory," *Appl. Phys. Lett.* **95**(13), 133503 (2009).
22. X. M. Wang, M. Kuwahara, K. Awazu, P. Fons, J. Tominaga, and Y. Ohki, "Proposal of a grating-based optical reflection switch using phase change materials," *Opt. Express* **17**(19), 16947–16956 (2009).
23. D. Tanaka, Y. Ikuma, Y. Shoji, M. Kuwahara, X. Wang, K. Kintaka, H. Kawashima, and H. Tsuda, "Demonstration of 1000-times switching of phase-change optical gate with Si wire waveguides," *Electron. Lett.* **46**, 1460 (2010).
24. T. Shintani, Y. Anzai, H. Minemura, H. Miyamoto, and J. Ushiyama, "Nanosize fabrication using etching of phase-change recording films," *Appl. Phys. Lett.* **85**(4), 639–641 (2004).
25. C. H. Chu, M. L. Tseng, C. Da Shiue, S. W. Chen, H.-P. Chiang, M. Mansuripur, and D. P. Tsai, "Fabrication of phase-change Ge₂Sb₂Te₅ nano-rings," *Opt. Express* **19**(13), 12652 (2011).
26. Q. Guo, M. H. Li, Y. Li, L. P. Shi, T. C. Chong, J. A. Kalb, and C. V. Thompson, "Crystallization-induced stress in thin phase change films of different thicknesses," *Appl. Phys. Lett.* **93**(22), 221907 (2008).
27. K. Y. Yang, S. H. Hong, D. K. Kim, B. K. Cheong, and H. Lee, "Patterning of Ge₂Sb₂Te₅ phase change material using UV nano-imprint lithography," *Microelectron. Eng.* **84**(1), 21–24 (2007).
28. Y. Zhang, S. Raoux, D. Krebs, L. E. Krupp, T. Topuria, M. A. Caldwell, D. J. Milliron, A. Kellock, P. M. Rice, J. L. Jordan-Sweet, and H.-S. P. Wong, "Phase change nanodots patterning using a self-assembled polymer lithography and crystallization analysis," *J. Appl. Phys.* **104**(7), 074312 (2008).
29. C. H. Chu, C. Da Shiue, H. W. Cheng, M. L. Tseng, H.-P. Chiang, M. Mansuripur, and D. P. Tsai, "Laser-induced phase transitions of Ge₂Sb₂Te₅ thin films used in optical and electronic data storage and in thermal lithography," *Opt. Express* **18**(17), 18383–18393 (2010).
30. S.-W. Nam, T.-Y. Lee, J.-S. Wi, D. Lee, H.-S. Lee, K.-B. Jin, M.-H. Lee, H.-M. Kim, and K.-B. Kim, "Electron-beam lithography patterning of Ge₂Sb₂Te₅ nanostructures using hydrogen silsesquioxane and amorphous Si intermediate layer," *J. Electrochem. Soc.* **154**(9), H844–H847 (2007).
31. J. Bohandy, B. F. Kim, and F. J. Adrian, "Metal deposition from a supported metal film using an excimer laser," *J. Appl. Phys.* **60**(4), 1538–1540 (1986).
32. H. Shin, H. Kim, H. Lee, H. Yoo, J. Kim, H. Kim, and M. Lee, "Photoresist-free lithographic patterning of solution-processed nanostructured metal thin films," *Adv. Mater. (Deerfield Beach Fla.)* **20**(18), 3457–3461 (2008).
33. D. A. Willis and V. Grosu, "Microdroplet deposition by laser-induced forward transfer," *Appl. Phys. Lett.* **86**(24), 244103 (2005).
34. S. Zergioti, S. Mailis, N. A. Vainos, A. Ikiades, C. P. Grigoropoulos, and C. Fotakis, "Microprinting and microetching of diffractive structures using ultrashort laser pulse," *Appl. Surf. Sci.* **138–139**(1-2), 82–86 (1999).
35. D. P. Banks, C. Grivas, J. D. Mills, R. W. Eason, and I. Zergioti, "Nanodroplets deposited in microarrays by femtosecond Ti:sapphire laser induced forward transfer," *Appl. Phys. Lett.* **89**(19), 193107 (2006).
36. A. I. Kuznetsov, R. Kiyon, and B. N. Chichkov, "Laser fabrication of 2D and 3D metal nanoparticle structures and arrays," *Opt. Express* **18**(20), 21198–21203 (2010).
37. M. Colina, M. Duocastella, J. M. Fernandez-Pradas, P. Serra, and J. L. Morenza, "Laser-induced forward transfer of liquids: Study of the droplet ejection process," *J. Appl. Phys.* **99**(8), 084909 (2006).
38. P. Serra, M. Duocastella, J. M. Fernandez-Pradas, and J. L. Morenza, "Liquids microprinting through laser-induced forward transfer," *Appl. Surf. Sci.* **255**(10), 5342–5345 (2009).
39. M. Colina, P. Serra, J. M. Fernández-Pradas, L. Sevilla, and J. L. Morenza, "DNA deposition through laser induced forward transfer," *Biosens. Bioelectron.* **20**(8), 1638–1642 (2005).
40. T. V. Kononenko, P. Alloncle, V. I. Konov, and M. Sentis, "Laser transfer of diamond nanopowder induced by metal film blistering," *Appl. Phys., A Mater. Sci. Process.* **94**(3), 531–536 (2009).
41. E. Fogarassy, C. Fuchs, F. Kerherve, G. Hauchecorne, and J. Perriere, "Laser-induced forward transfer of high-Tc YBaCuO and BiSrCaCuO superconducting thin films," *J. Appl. Phys.* **66**(1), 457 (1989).
42. S. Mailis, I. Zergioti, G. Koundourakis, A. Ikiades, A. Patentalaki, P. Papakonstantinou, N. A. Vainos, and C. Fotakis, "Etching and printing of diffractive optical microstructures by a femtosecond excimer laser," *Appl. Opt.* **38**(11), 2301–2308 (1999).
43. M. C. Suh, B. D. Chin, M.-H. Kim, T. M. Kang, and S. T. Lee, "Enhanced luminance of blue light-emitting polymers by blending with hole-transporting materials," *Adv. Mater. (Deerfield Beach Fla.)* **15**(15), 1254–1258 (2003).
44. J. Lee and S. Lee, "Laser-induced thermal imaging of polymer light-emitting materials on poly(3,4-ethylenedioxythiophene): silane hole-transport layer," *Adv. Mater. (Deerfield Beach Fla.)* **16**(1), 51–54 (2004).
45. C. M. Chang, C. H. Chu, M. L. Tseng, H.-P. Chiang, M. Mansuripur, and D. P. Tsai, "Local electrical characterization of laser-recorded phase-change marks on amorphous Ge₂Sb₂Te₅ thin films," *Opt. Express* **19**(10), 9492–9504 (2011).

46. C. H. Chu, B. J. Wu, T. S. Kao, Y. H. Fu, H.-P. Chiang, and D. P. Tsai, "Imaging of recording marks and their jitters with different writing strategy and terminal resistance of optical output," *IEEE Trans. Magn.* **45**(5), 2221–2223 (2009).
47. S. K. Lin, I. C. Lin, and D. P. Tsai, "Characterization of nano recorded marks at different writing strategies on phase-change recording layer of optical disks," *Opt. Express* **14**(10), 4452–4458 (2006).
48. T. Nonaka, G. Ohbayashi, Y. Toriumi, Y. Mori, and H. Hashimoto, "Crystal structure of GeTe and Ge₂Sb₂Te₅ meta-stable phase," *Thin Solid Films* **370**(1-2), 258–261 (2000).
49. S. Danto, F. Sorin, N. D. Orf, Z. Wang, S. A. Speakman, J. D. Joannopoulos, and Y. Fink, "Fiber field-effect device via in situ channel crystallization," *Adv. Mater. (Deerfield Beach Fla.)* **22**(37), 4162–4166 (2010).

1. Introduction

Phase-change chalcogenide materials have special optical and electrical properties in their amorphous and crystalline states [1–4]. Among the numerous phase-change materials, Ge₂Sb₂Te₅ is typical with its short transition time, high thermal stability, large contrast of conductivity and reflectance between different phase states, and nearly completed reversible phase-change properties [5–7]. Also, some researches point out other interesting properties of Ge₂Sb₂Te₅ such as partial crystallization and electrolytic switching (polarity-dependent resistance). Optical and/or electronic multi-levels of Ge₂Sb₂Te₅ structures can be engineered through careful modulation of the input energy for phase transition [8–14].

Among the applications of Ge₂Sb₂Te₅, high-density optical data storage [3,15–18], phase-change electrical memory [7,19–21], and phase-change device [22–26] are some of the useful applications that have emerged in recent years. For patterning Ge₂Sb₂Te₅ some techniques are proposed, but most of the processes are complex, expensive, and time-consuming [27–30]. A production method with high efficiency and simplicity for Ge₂Sb₂Te₅ is needed. Laser-induced forward transfer (LIFT) technique is a versatile and high-throughput fabrication method. A range of materials has been patterned by the LIFT technique such as metals [31–36], materials in liquid state [37,38], biomaterials [39], diamond powder [40], superconductor [41], InOx [42], and various polymers [43,44]. The main idea behind LIFT is energy transformation, in which the optical energy of laser pulses is transformed into the kinetic energy of the forward transferred donor material. A schematic illustration of the LIFT setup is shown in Fig. 1. The laser beam passes through the supporting transparent substrate and focuses on the pre-coated thin film (called donor), creating an expansive pressure at the interface between the film and the substrate. The donor material melts and expands during illumination until the pressure goes over a threshold to detach and transfer the material. The local material is thus ablated forward and deposited onto the opposite substrate (called receiver). Because LIFT is a laser-direct-writing process, the required experimental setup is fairly simple and operation is low-cost. There is no need for a clean room, chemical compounds, and vacuum chambers. Most of the LIFT processes are carried out under ambient atmospheric conditions. This simple, fast, one-step technique has great application potential in research on micro- and nano-device fabrication.

In this paper, we report a process to fabricate phase-change Ge₂Sb₂Te₅ dots by utilizing the LIFT process. Fabrication of the Ge₂Sb₂Te₅ patterns is carried out with different laser fluences and with different thicknesses of the donor film. The electrical properties of LIFT dots are investigated by conductive-tip atomic force microscopy (C-AFM), which is an ideal tool for characterizing this particular class of materials [45–47]. Both electrical and optical multi-levels of the LIFT dots are observed, and a three-dimensional partial crystallization model is proposed. To the best of our knowledge, this is the first report on patterning phase-change chalcogenide materials by the LIFT technique, showing the complex and interesting phase compositions of the resulting patterns due to opto-thermal interactions and the mass transfer inherent in the LIFT process.

2. Experimental

The as-deposited Ge₂Sb₂Te₅ films are sputtered on a transparent BK-7 glass (Matsunami cover glass, 22 × 22 mm², 0.15mm thickness) under Ar pressure of 5 × 10⁻¹ pa by a conventional magnetron sputtering machine (Shibaura Mechatronics Corporation). The

$\text{Ge}_2\text{Sb}_2\text{Te}_5$ thin film on glass substrate is treated as the “donor”. Another cover glass substrate acting as the “receiver” is placed on the donor substrate. The donor-receiver pair is mounted on the femtosecond laser lithography system, and a 100-nm-thick spacer is placed between them. A Ti:sapphire femtosecond laser (Coherent Inc., $\lambda = 800$ nm, pulse duration = 140 fs, repetition rate = 80 MHz) is used as a light source. An attenuator and a shutter with switching time of 30 ms are used for the control of the incident laser fluence and exposure time. The laser beam is expanded to a diameter of 6 mm by a spatial filter. A $\lambda/4$ wave plate transforms the laser beam into circular polarization. Finally the laser beam is focused by a high-numerical-aperture oil-immersion objective lens (Zeiss Plan-Apochromat, 100 \times , 1.4NA, 0.17 mm working distance) through the transparent substrate on the $\text{Ge}_2\text{Sb}_2\text{Te}_5$ donor film. A charge coupled device (CCD) is used for real time monitoring. Subsequently, for the measurement of the optical reflectance of the transferred dots, an optical microscope (Leica MPV-SP, 50 \times , 0.5NA) is used to acquire an optical image (in reflection) for the analysis of reflectance.

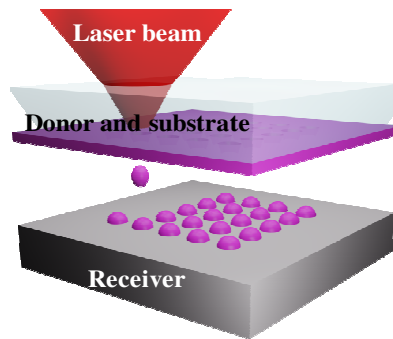


Fig. 1. Schematic illustration of the LIFT technique.

The C-AFM (Asylum Research, MFP-3DTM) measurement scheme is depicted in Fig. 2a; the microscope is operated in contact mode. The C-AFM applies a bias voltage of 1.5 V to the ITO film of the receiver, and the local conductance is obtained by recording the current passing through the conductive probe. The contact-mode C-AFM probe is coated with a 15 nm-thick layer of PtIr₅ for electrical measurements, as shown in Fig. 2b.

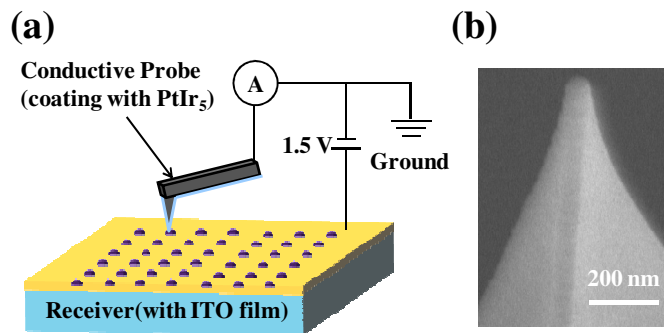


Fig. 2. (a) Schematic illustration of the C-AFM measurement. (b) Magnified SEM image of the C-AFM probe.

3. Results and discussions

Figure 3 shows AFM images of 80-nm-thick as-deposited $\text{Ge}_2\text{Sb}_2\text{Te}_5$ donor film (Fig. 3a), the corresponding receiver (Fig. 3b), and the zoom-in images (Figs. 3c to 3e). The interspace between adjacent dots is 5 μm , and the laser fluence is varied from 9 to 90 mJ/cm^2 for each row. In Fig. 3a, bumps (9 mJ/cm^2) and holes (18 to 90 mJ/cm^2) surrounded by depressed rings

are observed on the donor. The average depth of the rings is about 5 nm, and the diameters increase with laser fluence. Ring formation is due to the phase transition from the as-deposited (essentially amorphous) state to the crystalline state of $\text{Ge}_2\text{Sb}_2\text{Te}_5$, which is accompanied with some density variation [29]. As shown in Fig. 3c, bumps are formed at the center of the laser spot, which originates from the redistribution of the molten material from the edge to the center of the illuminated region [25,29,45]. The height and the diameter of the bump are about 15 nm and 800 nm, respectively; the 9 mJ/cm^2 fluence is considered as the threshold of film ablation. In the fluence regime of 18–90 mJ/cm^2 , the diameter of the ablated holes varies linearly from 1.5 to 2 μm —the ablated parts of the donor are transferred to the receiver.

As shown in Fig. 3b, different $\text{Ge}_2\text{Sb}_2\text{Te}_5$ dots or rings found on the receiver depend on laser fluence. The configurations and features of LIFT $\text{Ge}_2\text{Sb}_2\text{Te}_5$ dots and rings are divided into three categories. The observed dot of first category is fabricated with the laser fluence of 9 mJ/cm^2 . The formation of dot array on the receiver is spotty and incomplete at this threshold energy for mass-transfer, and the corresponding pattern on donor is not an ablated hole but a bump structure. As shown in Fig. 3d, the height and diameter of the transferred dots are around 4.5 nm and 2.0 μm , respectively.

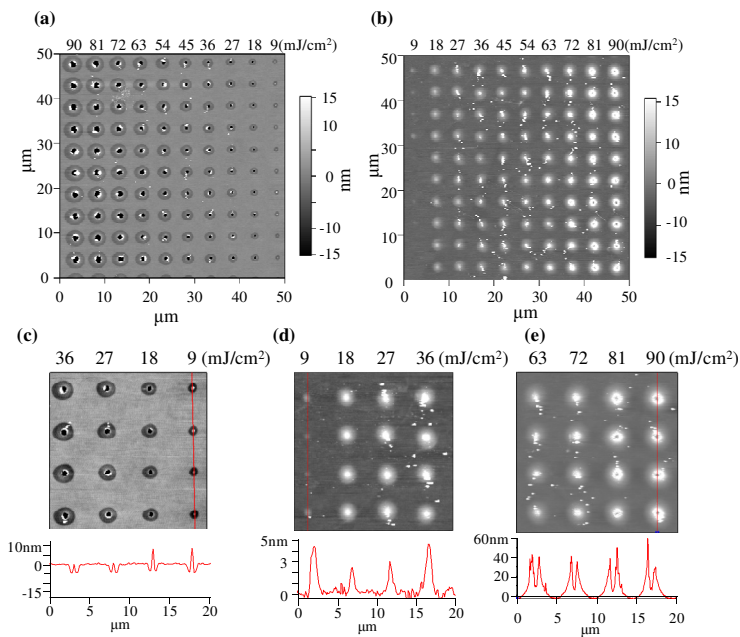


Fig. 3. (a) AFM image of the donor film (80-nm-thick as-deposited $\text{Ge}_2\text{Sb}_2\text{Te}_5$) exposed to different laser fluences. (b) AFM image of the corresponding receiver film. (c) Magnified AFM image of the donor and the corresponding cross-sectional profile (red line) under the laser fluence of 9–36 mJ/cm^2 ; bumps appear at 9 mJ/cm^2 . (d) and (e) Magnified AFM images of the receiver under laser fluences of 9–36 mJ/cm^2 and 63–90 mJ/cm^2 , respectively; LIFT dots and rings can be seen on the receiver. The corresponding cross-sectional profiles of the dots/rings are displayed below each AFM image.

Dots formed in the laser fluence regime of 18–72 mJ/cm^2 belong to the second category. In this category, completed dots are observed on the receiver surface. The size of these dots increases with an increasing laser fluence, the minimum dot diameter being $\sim 2.2 \mu\text{m}$. A significant amount of debris (on the order of tens of nanometers in diameter) is found on the receiver surface, which is made of quenched $\text{Ge}_2\text{Sb}_2\text{Te}_5$ material. The debris formation may be due to the fact that the $\text{Ge}_2\text{Sb}_2\text{Te}_5$ material is transferred as a mixture of solid and liquid phases.

In the third category, rings are formed in the fluence regime of 81 to 90 mJ/cm^2 . Figure 3e shows a magnified AFM image obtained in this regime. The inner and outer diameters of the

rings are approximately 1.5 μm and 3.0 μm , respectively. Rings are produced when the laser energy is well above the transfer threshold, perhaps because of the greater impact momentum and lower surface tension of the material during landing and cooling; this is similar to the results reported in Ref. [35].

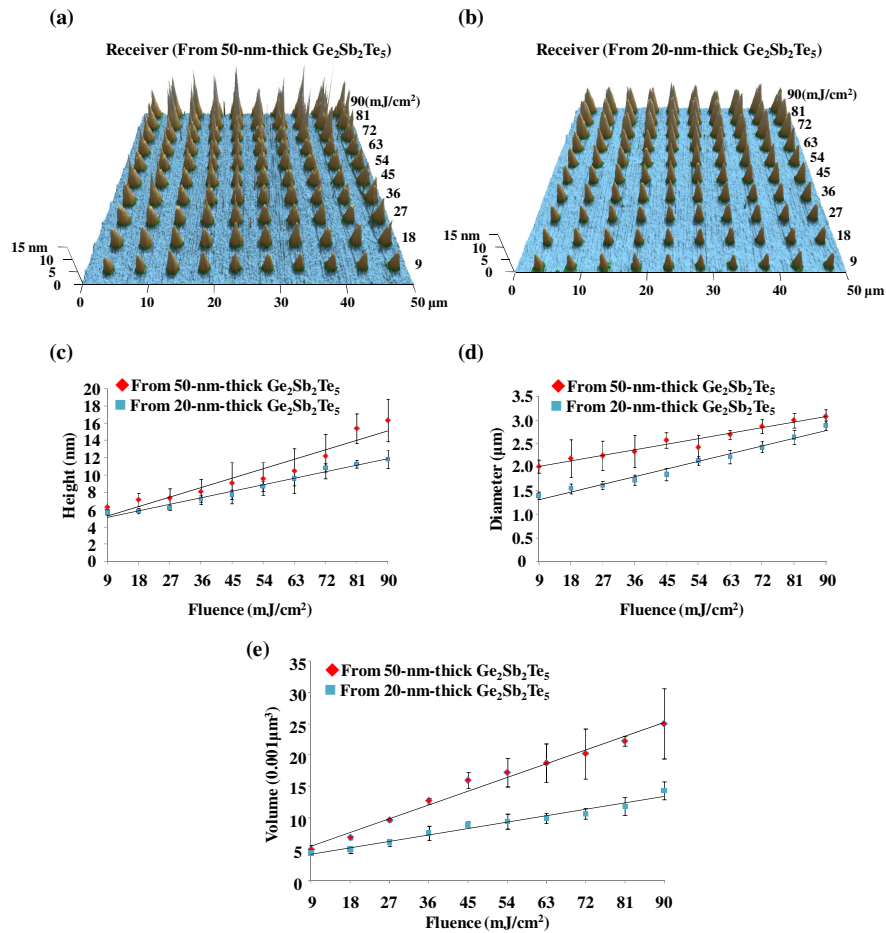


Fig. 4. (a) and (b) Three-dimensional AFM images of LIFT dots for 50-nm-thick and 20-nm-thick Ge₂Sb₂Te₅ donor films, respectively. (c)-(e) AFM measurements of height, diameter, and volume of LIFT dots as functions of laser fluence for donor films of differing thickness.

Figures 4a and 4b are three-dimensional AFM images of the LIFT dots transferred respectively from the 50-nm-thick and 20-nm-thick Ge₂Sb₂Te₅ donor films. The dots in these images are seen to be uniform, their sizes varying in proportion to the laser fluence. The debris is absent from the receiver surfaces, which could indicate that the Ge₂Sb₂Te₅ material is transferred in the liquid phase. Therefore, to prevent the formation of transferred debris on the receiver, it appears that the thickness of the Ge₂Sb₂Te₅ donor film should be less than about 50 nm. Comparing Figs. 4a and 4b, one observes that, at a given laser fluence, the dots transferred from the 50-nm-thick donor film are larger than those obtained from the 20-nm-thick donor. The AFM-measured values of the dot size (height, diameter, and volume) from different donor films (50 or 20-nm-thick Ge₂Sb₂Te₅) are plotted against laser fluence in Figs. 4c to 4e. The size is seen to be linearly proportional to the laser fluence in the range of 9-90 mJ/cm² with a step of 9 mJ/cm². The minimum height and diameter of the LIFT dots are about 5.7 nm and 1.4 μm for the 20-nm-thick Ge₂Sb₂Te₅ thin film. The minimum average volume of the LIFT dots is found from AFM measurements to be around $4.4 \times 10^{-3} \mu\text{m}^3$. The smallest

transferred mass under 9 mJ/cm^2 laser fluence is estimated at around 25.6 femtograms [48]. For the 50-nm-thick donor film, a clear deviation of the transferred dot height from linear dependence on the laser fluence can be seen in Fig. 4c. This deviation from linearity of the AFM-measured values for the 50-nm-thick $\text{Ge}_2\text{Sb}_2\text{Te}_5$ donor film may be attributed to the large impact momentum of the relatively massive transferred dot.

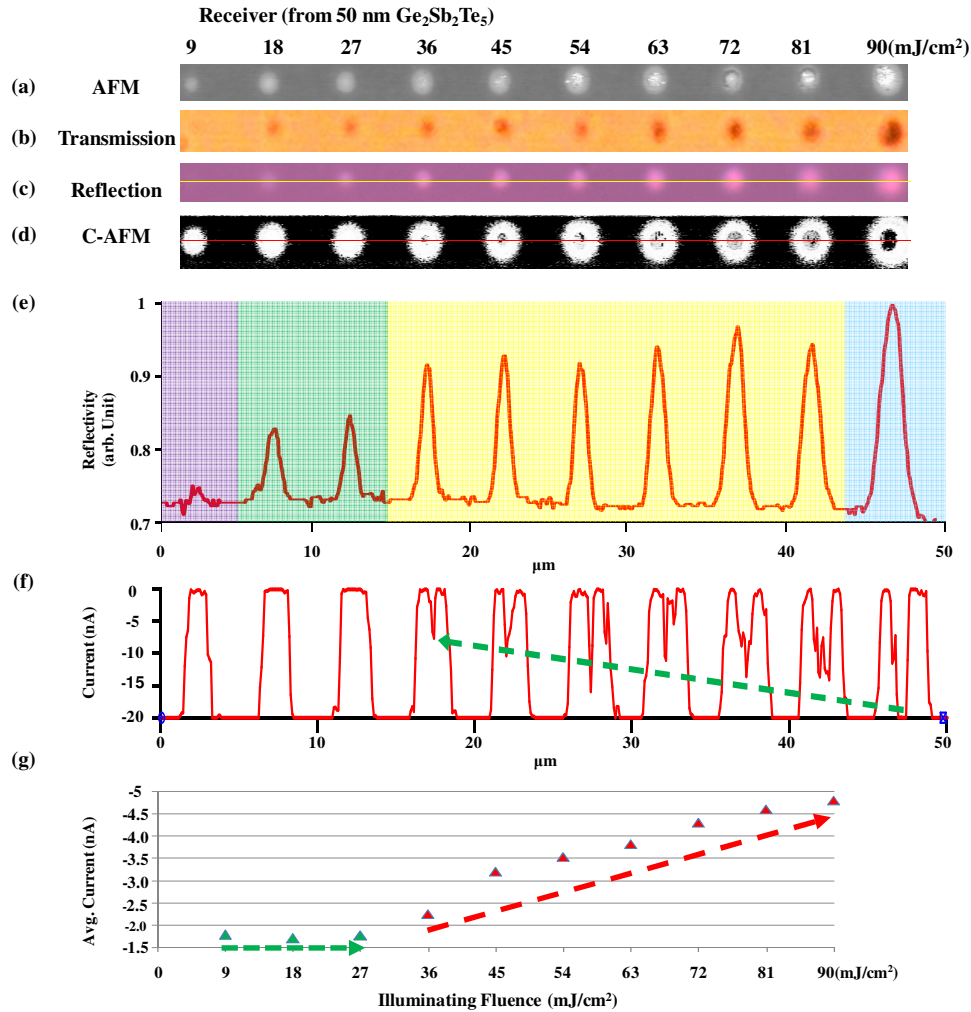


Fig. 5. (a)-(d) AFM, optical transmission, optical reflection, and C-AFM images of LIFT dots obtained from a 50-nm-thick as-deposited $\text{Ge}_2\text{Sb}_2\text{Te}_5$ donor. The four images are shown on the same scale. (e) Cross-sectional profile of LIFT dots extracted from the reflection optical-micrograph. Background color indicates different states. (f) Cross-sectional profiles of LIFT dots extracted from the C-AFM images—the arrow points to the conductivity at the center of the dot. (g) Average current passing through each LIFT dot as a function of laser fluence.

The mechanism of crystallization of the once molten $\text{Ge}_2\text{Sb}_2\text{Te}_5$ is believed to be formation and growth of nano-crystalline grains [8–11,45]. To understand the crystallization behavior of the $\text{Ge}_2\text{Sb}_2\text{Te}_5$ dots fabricated by the LIFT process, we compare in Fig. 5 their topography as well as their optical and electrical characteristics. The donor is the 50-nm-thick as-deposited $\text{Ge}_2\text{Sb}_2\text{Te}_5$ film, while the receiver is a BK-7 glass slide coated with a 12-nm-thick indium-tin-oxide (ITO) film, which is used as bottom electrode for C-AFM measurements. The AFM and transmission optical micrographs are shown in Figs. 5a and 5b, respectively. Transmittance of the LIFT dots is seen to vary with laser fluence. The phase-

state of the dots may be inferred from the optical contrast of the $\text{Ge}_2\text{Sb}_2\text{Te}_5$ material [5,29]. The dot transferred with 9 mJ/cm^2 is believed to be amorphous because of its high transmittance. The low-transmittance dots (formed in the regime of 18 to 90 mJ/cm^2) appear to contain nucleated fine crystallites. Figures 5c and 5e show the reflection optical-micrograph and its corresponding cross-sectional profile. Reflectance of the dots is seen to increase with the laser fluence in the regime of 18– 90 mJ/cm^2 . The cross-sectional profiles exhibit a four-level reflectance, occurring at the laser fluences of 9 mJ/cm^2 , 18– 27 mJ/cm^2 , 36– 81 mJ/cm^2 , and 90 mJ/cm^2 ; these various reflection levels are attributable to different degrees of crystallinity of $\text{Ge}_2\text{Sb}_2\text{Te}_5$. The presence of a reflectance gradient is clear evidence that the crystalline fraction of the LIFT dots primarily depends on laser fluence. However, considering that for different thicknesses of the $\text{Ge}_2\text{Sb}_2\text{Te}_5$ donor film, the mass and the shape of the transferred dots are dissimilar, the detailed behavior of the transferred $\text{Ge}_2\text{Sb}_2\text{Te}_5$ during the process of cool-down and crystallization is expected to be different as well.

Figure 5d is the C-AFM image of the corresponding dots. The regions displayed in white color are the low conductivity areas of the $\text{Ge}_2\text{Sb}_2\text{Te}_5$ material, which is considered to be amorphous. The LIFT dots observed in C-AFM image can be divided into two categories. In the first category, LIFT dots fabricated with fluence from 9 to 27 mJ/cm^2 show relatively low conductivity, and they may be considered as amorphous. LIFT dots in the second category, created under laser fluences of 36– 90 mJ/cm^2 , display a conductive area in the middle, where the GST material is either fully or partially crystalline. The non-conductive ring surrounding the conductive center of each LIFT dot is believed to be in the melt-quenched amorphous state. In this category, the conductive area of the LIFT dot gradually changes with increased laser fluence from light-gray to dark, indicating an increase of conductivity (i.e., density of crystalline grains) with laser fluence.

The LIFT dots in the C-AFM image show larger diameters than the corresponding ones in the AFM and optical microscopic images. This indicates the presence of amorphous $\text{Ge}_2\text{Sb}_2\text{Te}_5$ regions around LIFT dots, and these extremely-thin regions are transparent. The highly sensitive electrical measurements by C-AFM provide excellent contrast for the conductivity of this amorphous region [45–47]. Figure 5f is the corresponding cross-sectional profile of the C-AFM image. These experimental data indicate that the change of the central conductive region is closely related to the laser fluence.

Comparing Figs. 5c and 5d, we note that the LIFT dots fabricated with a fluence of 9 mJ/cm^2 , having poor conductivity and low reflectance, are predominantly amorphous. The LIFT dots obtained with a fluence of 18 to 27 mJ/cm^2 are also weakly conductive, similar to the dots obtained with a 9 mJ/cm^2 fluence, but the optical reflectance of these dots is higher than the background. We consider that the dots transferred by 18 to 27 mJ/cm^2 are dominantly amorphous $\text{Ge}_2\text{Sb}_2\text{Te}_5$ mixed with some crystalline grains. Moreover, the high-conductivity areas of the LIFT dots shown in Fig. 5d in the regime of 36 to 90 mJ/cm^2 are somewhat smaller than those of the corresponding high-reflectance LIFT dots shown in Fig. 5c, which indicates that the optical contrast for the observation of partially crystallized regions is better than the electrical conductivity of C-AFM.

We summarize our observations as follow: with enough laser fluence, crystalline grains are formed in the central regions of each LIFT dot. The distribution of crystalline grains is locally different for each dot; also dot density varies with the transfer fluence. When the receiver is subjected to an electric field, filamentary pathways form within the dots that contain a sufficient number of crystalline grains, thus allowing electrical currents to flow from the conductive AFM probe through the receiver. Variations of conductivity and reflectance originate from the various densities of crystalline grains within the dot. Figure 5(g) shows the average C-AFM currents of dots formed with different laser fluences, and the electrical states of dots can be divided into two regimes: 9 to 27 mJ/cm^2 and 36 to 90 mJ/cm^2 . The average C-AFM current in the first regime is -1.74 nA ; this constant value of the average current may be due to the dominantly amorphous nature of the receiver dots. The average C-AFM currents of the dots in the second regime are nearly linear functions of the transfer fluencies, varying from -2.2 nA to -4.8 nA .

The LIFT technique can fabricate designed patterns on arbitrary receivers such as flexible transparency sheets [32] and optical fibers [34,42]. For these novel applications of phase-change chalcogenides, complex structures can be fabricated by the LIFT technique with high efficiency. We demonstrate in Fig. 6 the fabrication of a reduction venation pattern as a biomimetic structure on a BK-7 glass substrate. In the original image file of the real leaf shown in Fig. 6a, the length and width of the leaf are around 6.8 cm and 4.7 cm, respectively; the picture is imported into a figure file for data processing. As shown in Fig. 6b, the image of leaf is turned into monochromatic form (302×195 pixels), and the leaf veins are picked out. We set the laser fluence to 63 mJ/cm^2 , the interspace between adjacent pixels to 250 nm, and chose a 20-nm-thick $\text{Ge}_2\text{Sb}_2\text{Te}_5$ film as donor. Figure 6(c) shows three-dimensional AFM images of the donor and the corresponding receiver. The size of the reduced veins structure is around $75 \times 31 \mu\text{m}^2$. The reduced venation pattern is complete and clean. Possible applications for this kind of venation pattern are control of optical splitter and electrical shunt, such as used in the field effect devices for optical fibers [49].

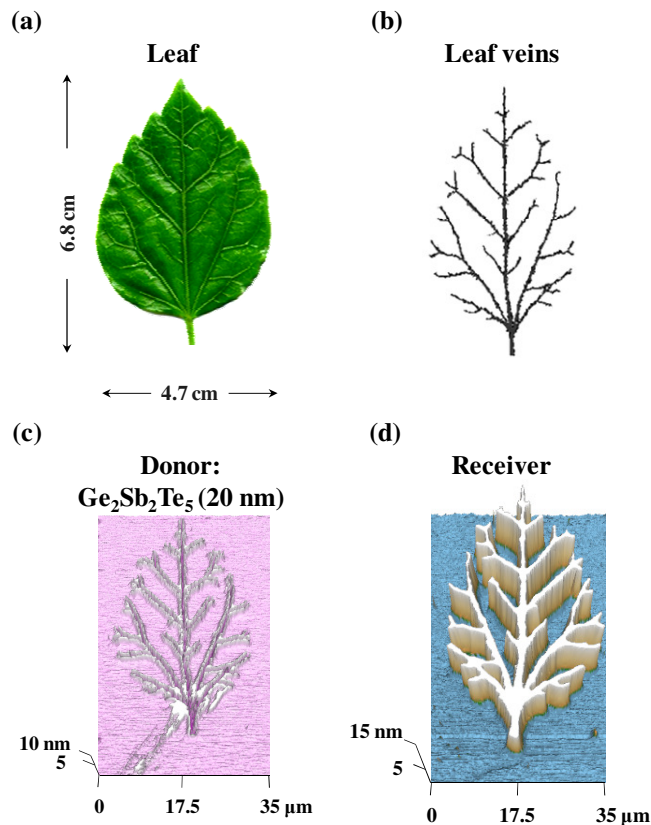


Fig. 6. Fabrication of the venation pattern. (a) Optical image of real leaf. (b) Monochrome image of venation. (c), (d) Three-dimensional AFM images of donor and receiver.

4. Conclusion

Patterned samples of the chalcogenide phase-change material $\text{Ge}_2\text{Sb}_2\text{Te}_5$ were fabricated and analyzed utilizing a femtosecond-laser-induced forward transfer process. The size, shape, and phase state of the transferred dots obtained in this LIFT process could be controlled by the laser fluence and by the thickness of the donor film. Our experiments show that the smallest mass transferred from a 50-nm-thick $\text{Ge}_2\text{Sb}_2\text{Te}_5$ film is about 25.6 femtograms. The multi-level optical and electrical states observed in our optical and C-AFM measurements have their

origins in the differing densities of the $\text{Ge}_2\text{Sb}_2\text{Te}_5$ crystalline grains. The non-uniform distribution of crystalline grains within each $\text{Ge}_2\text{Sb}_2\text{Te}_5$ dot (revealed by C-AFM measurements) plays an important role in the electro-optical properties of the LIFT dots. To our knowledge, this is the first report on the fabrication of phase-change material structures by the LIFT process. Our results have potential for application in the areas of optically- and/or electrically-switchable phase-change devices.

Acknowledgments

The authors thank the National Science Council, Taiwan, for the financial support of this project under grant numbers 99-2911-I-002-127 and 99-2120-M-002-012. They also thank the Molecular Imaging Center of the National Taiwan University for technical support.